NIR Emitting Scintillators Based on CsI Single Crystals

Veronika Gavrilenko , Viktorija Pankratova , Vladimir Pankratov , Ekaterina Kaneva , Roman Shendrik , Dmitriy Sofich *

Posted Date: 30 April 2025

doi: 10.20944/preprints202504.2567.v1

Keywords: cesium iodide; scintillator; europium; ytterbium; samarium; luminescence; single crystal; crystal growth

 doi:10.20944/preprints202504.2567.v1

Article

NIR Emitting Scintillators Based on CsI Single Crystals

Dmitriy Sofich [1], Veronika Gavrilenko [1], Viktorija Pankratova [2], Vladimir Pankratov [2], Ekaterina Kaneva [1] and Roman Shendrik [1,*]

[1] Vinogradov Institute of Geochemistry, Irkutsk, 664033, Russia
[2] Institute of Solid State Physics, University of Latvia, 8 Kengaraga Iela, LV-1063 Riga, Latvia
* Correspondence: sofich@igc.irk.ru

Abstract: The development of efficient scintillators emitting in the red and/or infrared spectral range represents an important scientific challenge, as such materials could find numerous practical applications. This work studies newly grown CsI:Yb,Sm and CsI:Eu,Sm single crystals demonstrating red and infrared luminescence. We measured luminescence spectra in the visible and near-IR range, excitation spectra across visible, UV, VUV, and X-ray ranges, Raman absorption spectra, and thermoluminescence spectra. The results show that divalent europium and ytterbium ions can efficiently transfer excitation to samarium ions. The measured X-ray light yield reached 37,000 photons/MeV for CsI:Yb,Sm and 40,000 photons/MeV for CsI:Eu,Sm.

Keywords: cesium iodide; scintillator; europium; ytterbium; samarium; luminescence; single crystal; crystal growth

1. Introduction

Red-emitting scintillators represent a crucial class of materials capable of converting ionizing radiation energy into red and near-infrared luminescence. These materials are of significant interest for radiation monitoring, medical imaging, and high-energy physics, as their spectral characteristics closely match the sensitivity range of semiconductor photodetectors. Ultra-compact yet highly sensitive scintillator-photodetector assemblies could be particularly valuable for real-time dosimetry monitoring during radiation therapy[1–4]. Traditional scintillator materials often rely on trivalent rare-earth ions as activators; however, divalent samarium (Sm^{2+}) has emerged as a promising alternative for NIR emission[5,6]. Sm^{2+} exhibits characteristic 5d→4f transitions that result in strong emission in the red and NIR regions, making it suitable for applications requiring efficient light conversion at these wavelengths. Also, divalent samarium exhibits low self-absorption, which contributes to high light yield even at high activator concentrations[7]. However, the practical application of Sm^{2+}-activated scintillators can be limited by the need for efficient energy transfer mechanisms[8–10]. To address these limitation, sensitization strategies involving co-doping with other rare-earth ions such as ytterbium (Yb^{2+})[6,11] or europium (Eu^{2+}) have been explored[9,12]. Yb^{2+} and Eu^{2+} can act as efficient sensitizers, absorbing energy from the host lattice and transferring it to Sm^{2+} via energy transfer processes, thereby enhancing the overall scintillation efficiency. Our previous studies[13,14] of activated CsI single crystals have revealed that while samarium ions exhibit efficient red emission through $4f^5 5d^1 \rightarrow 4f^6$ transitions, their practical application is limited by poor spectral overlap between the host exciton emission band and Sm^{2+} absorption. Therefore, the luminescence of Sm^{2+} exhibits low intensity under X-ray excitation. However, co-doping with suitable sensitizers can enhance energy transfer and increase X-ray-excited luminescence. The optimal impurities for this co-doping strategy are Yb^{2+} and Eu^{2+}, as the energy transfer processes involving these activators are relatively efficient[13,15]. This article focuses on the development and characterization of novel scintillator materials based on CsI crystals activated with divalent samarium (Sm^{2+}) and sensitized with ytterbium

 doi:10.20944/preprints202504.2567.v1

(Yb^{2+}) or europium (Eu^{2+}). We explore the luminescence and scintillation properties of these materials under visible, near ultraviolet, synchrotron and X-ray excitation.

2. Materials and Methods

Granulated CsI with a purity of 99.998% (with respect to metal impurities), produced by Lanhit, was used as the starting material for crystal growth. The activators consisted of SmI_2 and YbI_2 powders, as well as granulated EuI_2, all with a purity of 99.99% (Lanhit). The initial mixture contained 150 g of CsI and 2.6 g of each activator (approximately 1 mol%). The materials were loaded into a vitreous carbon crucible inside the furnace and heated under vacuum at 500°C for six hours to remove adsorbed oxygen and moisture. By the end of the drying process, the residual vapor pressure in the furnace was below 0.01 Pa. The growth setup comprises a spherical water-cooled stainless steel chamber. A crystal pulling rod, thermostatically water-cooled and driven by two stepper motors, provides simultaneous rotation and vertical displacement of the growing crystal. A graphite adapter fitted with a quartz capillary is mounted at the rod 's extremity (Figure 1). The furnace is equipped with a cylindrical resistive heater surrounded by pyrolytic graphite thermal insulation. Temperature regulation is achieved using a K-type thermocouple fixed to the crucible base. To suppress melt evaporation, both melting and crystal growth were conducted in an argon atmosphere maintained at 110 kPa.

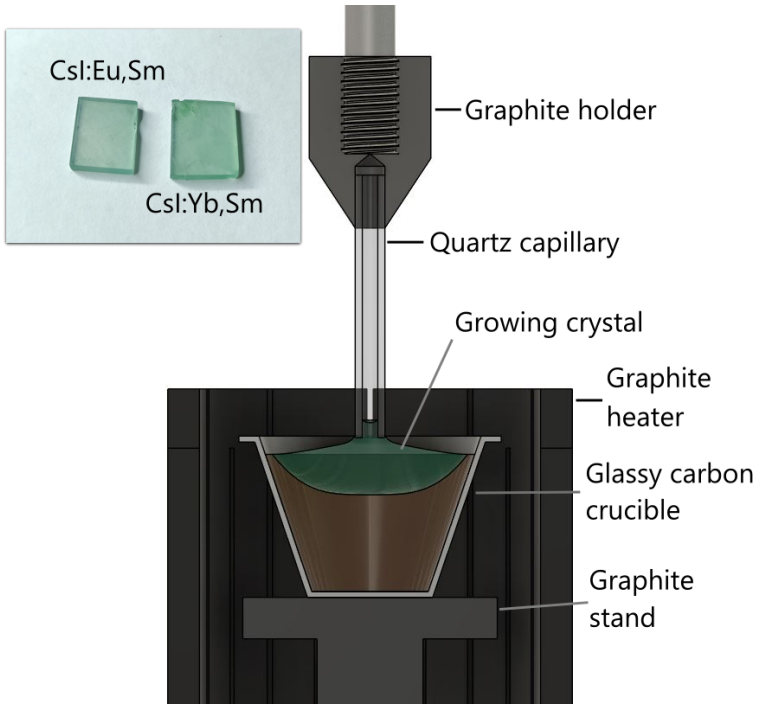

Figure 1. Schematic of the crystal growth setup and photographs of samples prepared for spectroscopic studies.

Crystal growth was initiated by seeding onto a quartz capillary. To grow the colored crystal, the Kyropoulos method was employed, which enables higher incorporation of dopant ions into the crystal lattice compared to the Czochralski technique. The crystal was grown at a cooling rate of 0.3°C/h. Although the Kyropoulos method typically involves crystal pulling and rotation from the melt, neither the pulling motor nor rotation were utilized in this case to maximize the dopant ion concentration in the as-grown crystal. As a result, a single crystal approximately 35 mm in diameter and 8 mm thick was obtained. It grew as a layer on the remaining part of the boule, where the melt began to solidify non-uniformly, exhibiting off-stoichiometry and inclusions of dendritic structures with unclear composition. This approach enables higher dopant concentrations but limits the growth of large, homogeneous crystals. Nevertheless, samples of sufficient quality for spectroscopic studies can still be cut from the resulting crystals. For comparative analysis, the spectra of CsI:Eu, CsI:Sm, and CsI:Yb

 doi:10.20944/preprints202504.2567.v1

crystals will be presented. These crystals were grown under identical conditions with similar activator concentrations. The luminescence and excitation spectra were registered by a spectrometer based on SDL-1 and MDR-2 grating monochromators (LOMO, Saint-Petersburg, Russia) equipped with a grating of 1200 and 600 lines per mm. A Hamamatsu H6780-04 photomultiplier module was used as a photodetector. Excitation was carried out using a high-pressure 150W xenon arc lamp DKSH-150 through an MDR-2 monochromator with a diffraction grating of 1200 lines/mm. Additionally, 405 and 450 nm lasers were used for excitation. A closed-cycle helium cryostat was used for studies in the temperature range of 7-300 K. The X-ray luminescence spectra were measured using an MDR-2 monochromator coupled with a cooled FEU-83 photomultiplier tube (S-1 photocathode type), under excitation by a 10L-01 X-ray tube operated at 50 kV voltage and 1 mA current. The luminescence experiments under VUV excitations were carried out using synchrotron radiation from 1.5 GeV storage ring of MAX IV synchrotron facility (Lund, Sweden). The luminescence experiments under synchrotron radiation excitations are a powerful tool for the study of scintillators[16,17]. The experiments have been performed at the photoluminescence endstation of FinEstBeAMS beamline. The parameters of the beamline and the experimental setup are given in[18]. The luminescence spectra were processed using an ArDI web-application (https://ardi.fmm.ru).

Raman spectra were measured using a WITec alpha300R confocal Raman spectrometer coupled with a 532 nm Nd:YAG laser at room temperature, calibrated on crystalline silicon. The spectra were recorded with a diffraction grating of 1800 lines per millimeter and a spectral resolution of 3 cm^{-1}. The laser beam had an output power of 10 mW, and the focal spot diameter sample was between 5 and 10μm. The backscattered Raman signal was collected by using a Zeiss 50x/NA 0.55 objective in a UHTS300 spectrometer equipped with a Peltier-cooled, front-illuminated CCD camera. Spectral scan durations were 20 s, with signals averaging over 5 scans.

3. Results

The undoped crystal does not exhibit Raman scattering due to its NaCl-type crystal lattice. However, Raman signals were detected in CsI crystals doped with 1 mol.% of Yb^{2+} and Sm^{2+}, as well as in those doped with 1 mol.% of Sm^{2+} and 1 mol.% of Eu^{2+}. The Raman spectra of these doped crystals are presented in Figure 2. The bands observed at 80, 94, 112, 136, and 164 cm^{-1} in the doped crystals can be attributed to $(Ln^{2+}I_8)^6$-vc clusters[19].

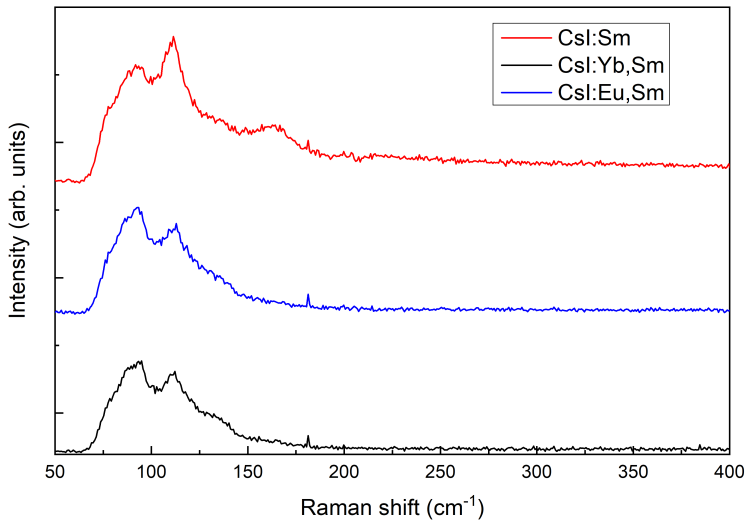

Figure 2. Raman absorption spectra of CsI:Sm (1); CsI:Yb,Sm (2) and CsI:Eu,Sm (3).

The luminescence spectra of CsI:Yb,Sm shown in Figure 3 were measured at temperatures of 298 K and 7 K. At room temperature, a band corresponding to the $4f^55d^1 \rightarrow 4f^6$ luminescence of divalent samarium[20] is observed in the red and infrared spectral regions, with a maximum intensity in the range of 1.4-1.5 eV (≈827-886 nm) under 405 nm laser excitation. In the long-wavelength region, the

 doi:10.20944/preprints202504.2567.v1

edge of the $4f^5 5d^1 \rightarrow 4f^6$ emission band is truncated due to the declining sensitivity of the detector used. In the blue spectral region at room temperature, two bands (high-spin and low-spin) of $4f^{13} 5d^1 \rightarrow 4f^{14}$ luminescence from divalent ytterbium ions are visible[21]. However, the emission intensity in these bands is two orders of magnitude lower than that of the divalent samarium band.

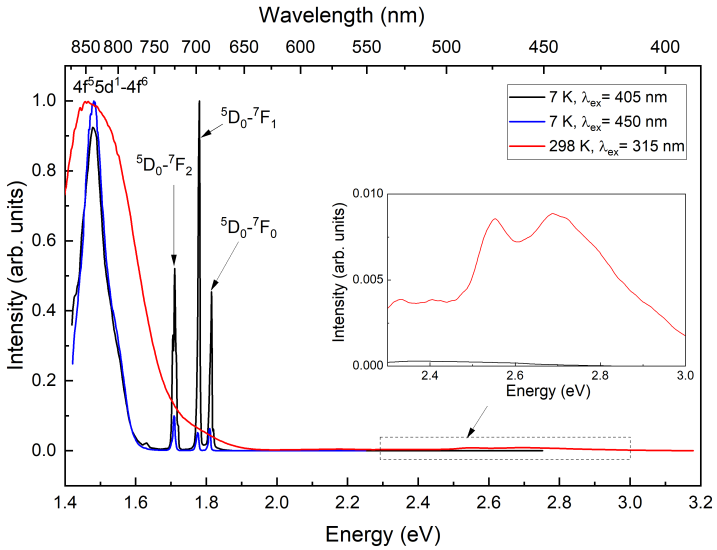

Figure 3. Luminescence spectra of CsI:Yb,Sm measured at 298 K and 7 K.

Upon cooling, the characteristic Yb^{2+} emission band nearly completely loses its intensity, while the $4f^5 5d^1 \rightarrow 4f^6$ emission band narrows, revealing a shoulder at 1.55 eV (≈800 nm). Additionally, $4f^6 \rightarrow 4f^6$ luminescence bands characteristic of divalent samarium ions appear[22,23], with observed transitions $^5D_0 \rightarrow {}^7F_0$, $^5D_0 \rightarrow {}^7F_1$ and $^5D_0 \rightarrow {}^7F_2$ showing maxima at 1.81 eV (≈685 nm), 1.77 eV (≈700 nm), and 1.71 eV (≈725 nm), respectively. When excited at 450 nm within the ytterbium emission band, the intensity of the $4f^5 5d^1 \rightarrow 4f^6$ emission increases significantly relative to the $4f^6 \rightarrow 4f^6$ transitions.

The excitation spectrum (Figure 4) consists of $4f^n 5d^1 \rightarrow 4f^n$ electronic transitions of Yb and Sm ions. In the region of $4f^6 \rightarrow 4f^6$ transitions of samarium, the main excitation bands show good agreement with the excitation bands of the reference CsI:Yb sample[13]. In the $4f^5 5d^1 \rightarrow 4f^6$ emission band of samarium ions, the excitation spectrum exhibits some anticorrelation compared to the excitation spectrum of $4f^6 \rightarrow 4f^6$ luminescence, suggesting different types of samarium emission centers responsible for $4f^6 \rightarrow 4f^6$ and $4f^5 5d^1 \rightarrow 4f^6$ luminescence.

The luminescence of the CsI:Eu,Sm sample (Figure 5) at room temperature consists of a broadened $4f^5 5d^1 \rightarrow 4f^6$ Sm^{2+} emission band, compared to CsI:Yb,Sm. Both CsI:Yb,Sm and CsI:Eu,Sm exhibit nearly identical $4f^6 \rightarrow 4f^6$ luminescence band profiles, indicating that the Sm^{2+} centers responsible for this emission experience similar crystal field environments. The $4f^6 5d^1 \rightarrow 4f^7$ Eu^{2+} emission band, peaking at 2.67 eV (≈464 nm)[24], also exhibits low intensity. Under 2.75 eV (450 nm laser) excitation, the samarium emission band ($4f^5 5d^1 \rightarrow 4f^6$) broadens and develops a vibrational structure, the energy spacing between these vibrational maxima falls within the 210-280 cm^{-1} range, that corresponds to doubled Raman frequency of divalent rare earth-iodine complexes (Figure 2). Upon cooling, four bands emerge in this spectral region, with maxima at 2.58 eV (≈481 nm), 2.66 eV (≈466 nm), 2.76 eV (≈449 nm), and 2.85 eV (≈435 nm).

The excitation spectrum (Figure 6) of CsI:Eu,Sm in the $4f^6 \rightarrow 4f^6$ luminescence band is completely identical to that of CsI:Yb,Sm in the $4f^6 \rightarrow 4f^6$ band. When exciting within the $4f^5 5d^1 \rightarrow 4f^6$ luminescence band of Sm ions, a certain correlation with the excitation spectrum of Eu^{2+} ions is observed. From the luminescence spectra, it is evident that both Eu and Yb act as sensitizers for Sm^{2+} ions.

 doi:10.20944/preprints202504.2567.v1

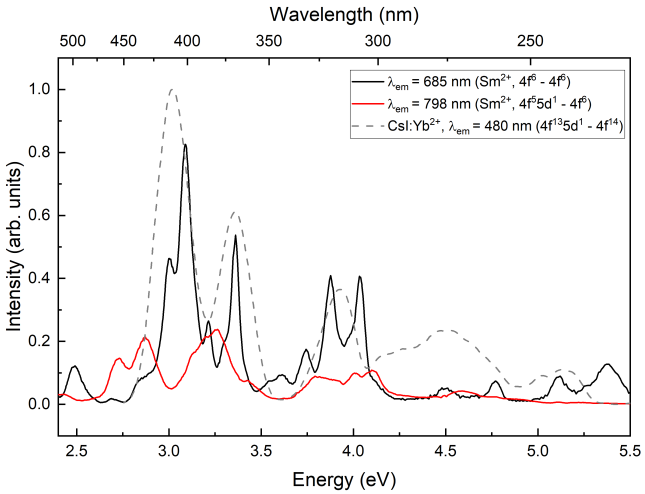

Figure 4. Excitation spectra of CsI:Yb,Sm measured at 7 K. The dashed line represents the excitation spectrum of CsI:Yb crystal measured at 298 K.

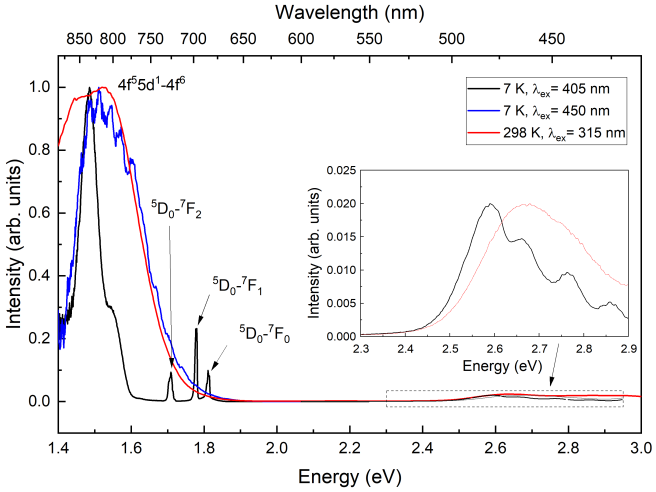

Figure 5. Luminescence spectra of CsI:Eu,Sm measured at 298 K and 7 K.

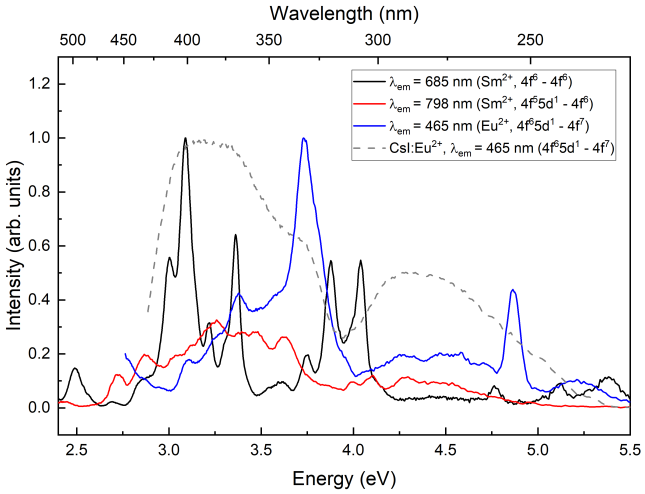

Figure 6. Excitation spectra in the $4f^6 \rightarrow 4f^6$ luminescence bands at 7 K.

 doi:10.20944/preprints202504.2567.v1

The excitation spectrum of CsI:Eu,Sm in the vacuum ultraviolet (VUV) region was measured in the $4f^6 \rightarrow 4f^6$ and $4f^5 5d^1 \rightarrow 4f^6$ emission bands at 7 K (Figure 7, curves (1) and (2)). A correlation is observed between the high-energy excitation spectra. In the 5-5.9 eV (≈248-210 nm) range, the $4f^6 \rightarrow 4f^6$ excitation spectrum exhibits two bands with maxima at 5.3 eV (≈234 nm) and 5.6 eV (≈221 nm), showing good correlation with the excitation spectrum of europium emission. In contrast, the $4f^5 5d^1 \rightarrow 4f^6$ band displays a broad continuum without characteristic dip. Notably, these excitation bands are absent in the $4f^5 5d^1 \rightarrow 4f^6$ excitation spectrum of CsI:Sm (Figure 7, curve 5). In the STE excitation region, the Eu^{2+} and Sm^{2+} crystals are not found intensive bands. However the similar to STE excitation bands structure could be observed (Figure 7, curves 2 and 3). In contrast, the only Sm^{2+} doped CsI crystal is not excited in the STE region (Figure 7, curve 5). The excitation spectrum in the $4f^6 5d^1 \rightarrow 4f^7$ band of CsI:Eu (Figure 8) correlates with the STE excitation spectrum, indicating an efficient energy transfer mechanism from self-trapped excitons to Eu^{2+} ions.

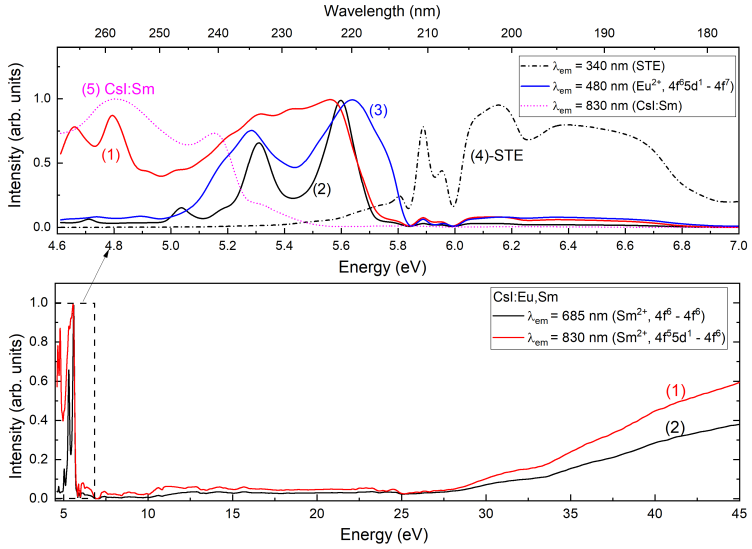

Figure 7. Excitation spectra of CsI:Eu,Sm and CsI:Sm (dot line) samples in VUV range.

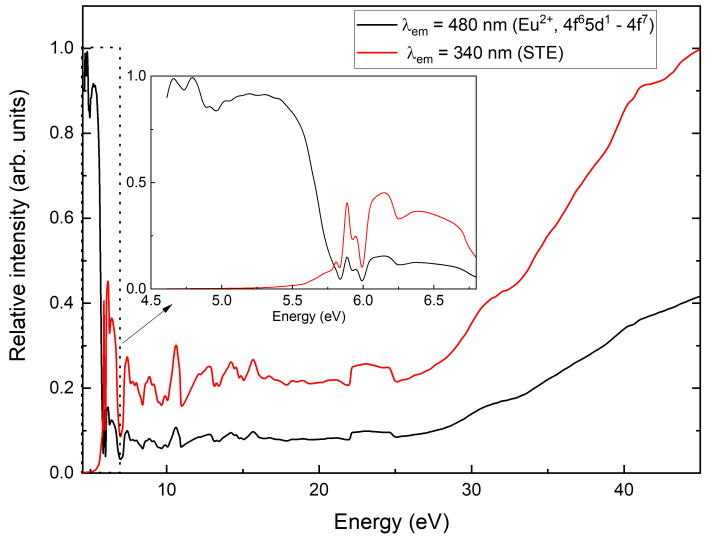

Figure 8. Excitation spectra of CsI:Eu in VUV range.

For a more detailed study of the divalent europium luminescence band, we measured the luminescence spectra of CsI:Eu crystals at 7 K under excitation at 5.6 eV (≈221 nm), 5.7 eV (≈218 nm), 5.3 eV (≈234 nm), and 3.7 eV (≈335 nm) (Figure 9). The Gaussian fitting analysis of the emission

 doi:10.20944/preprints202504.2567.v1

band demonstrates that the spectrum consists of five overlapping components with maxima at 2.69 eV (≈461 nm), 2.73 eV (≈454 nm), 2.78 eV (≈446 nm), 3.03 eV (≈409 nm), and 3.17 eV (≈391 nm). The relative intensities of these bands show significant variation with increasing excitation energy. Furthermore, the spectrum contains an additional luminescence peak at 3.66 eV (≈339 nm) corresponding to self-trapped exciton emission.

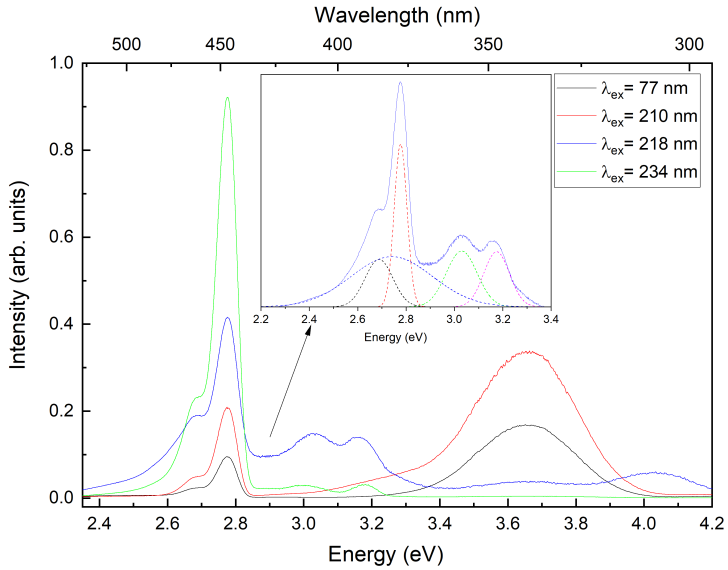

Figure 9. Luminescence spectra of CsI:Eu under VUV excitation at 7 K.

To determine the light yield, we measured the X-ray luminescence spectra (Figure 10) of the synthesized samples and a commercial CsI:Tl scintillator crystal (light yield: 54,000 photons/MeV) used as a reference. All samples were prepared with identical geometric dimensions. Given the broad spectral range of the emission bands, the measurements employed a cooled photomultiplier tube with a silver-oxygen-cesium (S-1 type) photocathode operating in pulse-counting mode. The recorded spectra were corrected for the instrument's spectral sensitivity. To verify that Eu and Yb ions act as effective sensitizers in scintillation process, we additionally measured the luminescence spectrum of a CsI:Sm crystal grown under the same conditions as the studied samples. The light yield and integrated emission intensity (expressed as a percentage relative to the reference) are summarized in Table 1. The measurement uncertainty of this method was 10%.

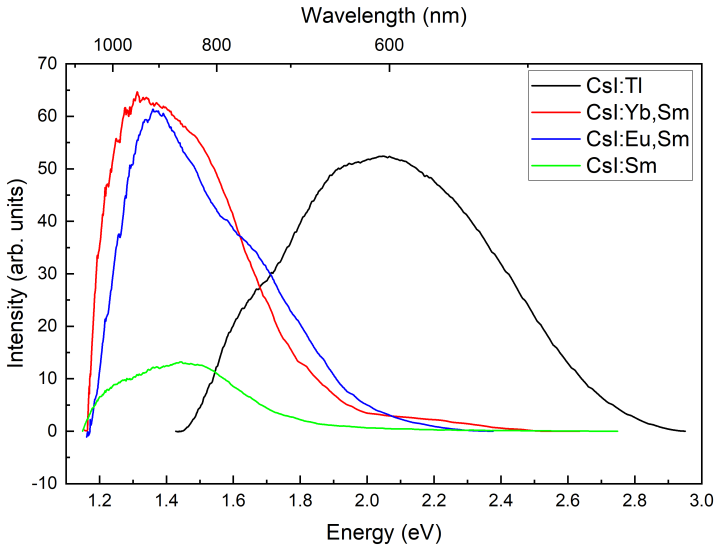

Figure 10. Luminescence spectra of CsI:Tl, CsI:Yb,Sm; CsI:Eu,Sm; and CsI:Yb,Sm crystals under X-ray excitation.

 doi:10.20944/preprints202504.2567.v1

Table 1. Light yield of samples under X-ray excitation.

Sample	Light yield relative to standard (%)	Light yield (photons/MeV)
CsI:Tl	100	54000[25]
CsI:Yb,Sm	68	36720
CsI:Eu,Sm	74	39960
CsI:Sm	14	7560

The thermoluminescence glow curves are given in Figure 11. The weak glow peaks at 125 and 140 K and intense glow peaks at 200, 255 and 275 K were observed in CsI:Yb, Sm crystals. In the crystals CsI: Eu, Sm the peaks at 205 and 290 K were observed.

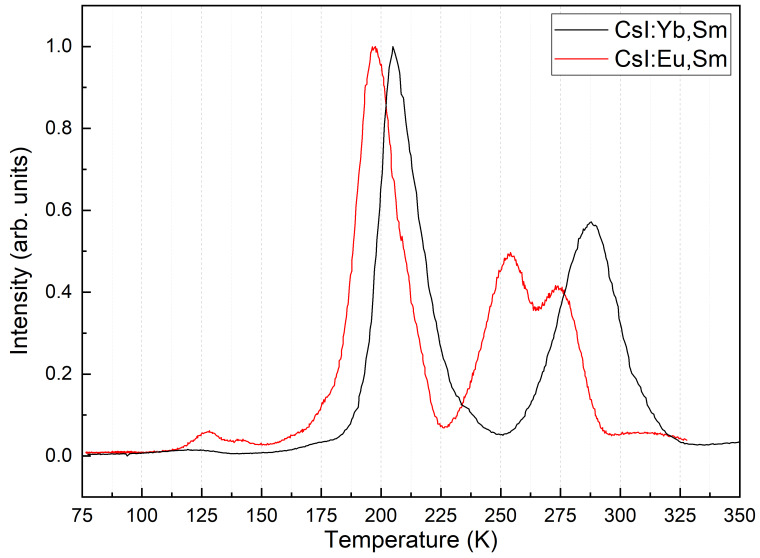

Figure 11. Thermoluminescence spectra of CsI:Yb,Sm and CsI:Eu,Sm.

4. Discussion

The most effective scintillators are materials in which energy transfer from intrinsic excitations to the activator ions occurs via excitons excitons[26–29]. In crystals activated by Yb^{2+}, this process also takes place, making them quite promising as scintillators[13].

In CsI-Eu crystals, the exciton mechanism is similarly observed[30,31], with the formation of near-impurity excitons also noted in these crystals. In the emission spectrum of Eu^{2+} in CsI crystals, excitation near the edge of the forbidden band reveals several bands. The broad band around 2.75 eV corresponds to the emission of a near-impurity exciton localized near sodium[32]. This band is also observed in unactivated, nominally impurity-free crystals. In europium-activated crystals, four additional bands appear at 2.7 eV, 2.77 eV, 3.00 eV, and 3.17 eV. Their excitation spectra differ from one another. The bands at 2.7 eV and 2.77 eV exhibit excitation bands in the 3 to 5 eV range, associated with intracenter excitation of 4f-5d transitions of Eu^{2+}[15,33]. Higher-energy bands are excited only within the energy range close to interband transitions of 5-5.6 eV. In the energy region where electron multiplications are observed, the luminescence bands at 2.7 eV and 2.77 eV are excited much more efficiently. Thus, these bands are associated with intracenter 5d-4f transitions in europium centers of different types is confirmed[30]. Such centers are most likely Eu^{2+} compensated by cation vacancies in nearest-neighbor (nn) and next-nearest-neighbor (nnn) positions. The nature of the higher-energy bands is likely associated with the decay of a near-impurity exciton near two types of Eu^{2+} centers. In this case, excitation transfer from these excitons to europium ions occurs, as indicated by an intense band in the 5-5.7 eV region observed in the excitation spectrum of 5d-4f europium luminescence (bands at 2.7 eV and 2.77 eV).

 doi:10.20944/preprints202504.2567.v1

From the excitation spectra of crystals with double activation (Figs. 6 and 7), it is evident that excitation transfer from the divalent ions of the sensitizers Eu^{2+} or Yb^{2+} to Sm^{2+} occurs. In particular, in crystals activated by europium, bands appear in the 5d-4f excitation spectrum in the 5.3 and 5.6 eV regions, associated with the excitation of a near-impurity exciton near europium[15] and weak bands in the region associated with self-trapped excitons at 5.9-6.0 eV. A similar pattern is observed in CsI-Yb, Sm crystals.

The energy transfer process is associated with the overlap of the emission bands of Eu^{2+} (Fig. 9) and Yb^{2+}[13] and the absorption characteristics of Sm^{2+}[14]. When excited in the 4f-5d bands of Yb^{2+} or Eu^{2+}, intense luminescence related to Sm^{2+} is observed, causing the entire volume of the crystal to glow. The intensity of 5d-4f luminescence from Sm^{2+} increases with rising concentrations of divalent lanthanide ions, as decreasing distances between Sm^{2+} ions and sensitizer ions (Yb^{2+} or Sm^{2+}) facilitate energy transfer. Thus, dipole-dipole nonradiative energy transfer from sensitizer ions Yb^{2+} or Eu^{2+} to Sm^{2+} ions presumably occurs.

In the excitation spectrum of 5d-4f luminescence, particularly within the region of interband transitions, coactivation of CsI-Sm^{2+} crystals with Yb^{2+} or Sm^{2+} ions reveals the occurrence of electron multiplications. This phenomenon suggests the establishment of an excitation transfer channel from the crystal lattice to Sm^{2+} ions, facilitated by the presence of Eu^{2+} and Yb^{2+} ions. Notably, a distinct band emerges in the 5d-4f excitation spectrum of Sm^{2+} luminescence, corresponding to a near-impurity exciton localized on either Eu^{2+} or Yb^{2+}. The precise origin of these excitons remains uncertain; however, it may be attributed to the deep energy states of Eu^{2+} and Yb^{2+} within the bandgap of CsI crystals, which could provide stability to the impurity exciton. Additionally, it is plausible that the decay of cationic excitons occurs at these impurity sites, as the core levels of Eu^{2+} and Yb^{2+} are situated within the energy range conducive to the formation of cationic excitons[34–36].

The thermoluminescence (TSL) bands in CsI-Yb, Sm and CsI-Eu, Sm crystals are associated with VkA hole centers near the divalent lanthanide ions. Since these bands differ between crystals with various sensitizers, they likely result from the nonradiative decay of a near-impurity exciton close to Yb^{2+} and Eu^{2+} ions. The TSL peaks in CsI-Eu, Sm crystals occur below room temperature, which means these crystals do not exhibit significant afterglow, unlike CsI-Tl crystals. In contrast, CsI-Yb, Sm crystals show a slight afterglow; however, this is several orders of magnitude less than that observed in CsI-Tl. Similarly, in CsI-Tl crystals co-activated with divalent lanthanides ions (Eu^{2+}, Yb^{2+} or Tm^{2+}), the afterglow intensity diminishes [37–40]. The light yield of the double-activated crystals was assessed using X-ray luminescence spectra, revealing a notable enhancement compared to crystals activated solely by Sm^{2+}. Specifically, CsI-Yb,Sm and particularly CsI-Eu,Sm crystals demonstrate great potential as scintillators emitting in the near-infrared region. Their light yield surpasses that of previously studied crystals[41] and may approach that of CsI-Tl.

5. Conclusions

For the first time, CsI crystals doubly activated with rare-earth ion pairs (Eu,Sm and Yb,Sm) have been successfully grown. Our studies demonstrate that divalent europium and ytterbium ions serve as efficient sensitizers for samarium ions (Sm^{2+}) in CsI crystals, where Sm^{2+} exhibits a broad 5d-4f emission band in the red and near-infrared spectral region. The light yield of the obtained crystals under X-ray excitation was evaluated to be approximately 37,000 photons/MeV for CsI:Yb,Sm and 40,000 photons/MeV for CsI:Eu,Sm. Further optimization of crystal growth techniques could significantly enhance the light output, potentially leading to the development of cost-effective infrared scintillators. These findings open new possibilities for creating efficient scintillation materials with emission in the near-infrared range.

Author Contributions: Conceptualization, D.S. and R.S.; methodology, D.S., R.S., V.P. (Vladimir Pankratov), V.P. and A.M.; validation, D.S., E.K., and V.P. (Vladimir Pankratov); formal analysis, V.P. (Viktorija Pankratova); investigation, D.S., R.S., V.G., V.P. (Vladimir Pankratov), V.P. (Viktorija Pankratova), and E.K.; resources, D.S.; writing—original draft preparation, D.S. and R.S.; writing—review and editing, V.P. (Vladimir Pankratov);

 doi:10.20944/preprints202504.2567.v1

visualization, D.S. and R.S.; supervision, D.S.; project administration, D.S. and V.P. (Vladimir Pankratov); funding acquisition, D.S. All authors have read and agreed to the published version of the manuscript.

Funding: This work (crystal growth and spectroscopy) was funded by the Russian Science Foundation (project No. 23-72-01097).

Data Availability Statement: The data presented in this study are available on request from the corresponding author. The Raman absorption spectra are available in the ArDI (Advanced spectRa Deconvolution Instrument) database – a web application designed for searching, processing, and analyzing vibrational spectra (https://ardi.fmm.ru/).

Acknowledgments: The synchrotron studies of CsI:Eu were conducted within the framework of State Assignment No. 0350-2016-0024 "Crystalline and Amorphous Functional Materials with Predictable Properties". The crystal growth facility utilizes equipment from the Isotope-Geochemical Research Shared Equipment Center at the Vinogradov Institute of Geochemistry (IGC SB RAS). Raman spectra were measured in Center for Geodynamics and Geochronology of Institute of Earth Crust SB RAS. V.P. acknowledges LZP grant lzp-2023/1-0063.

Conflicts of Interest: The authors declare no conflicts of interest. The funders had no role in the design of the study; in the collection, analyses, or interpretation of data; in the writing of the manuscript; or in the decision to publish the results.

Abbreviations

The following abbreviations are used in this manuscript:

NIR	Near-Infrared Light
VUV	Vacuum ultraviolet
UV	Ultraviolet
STE	Self-trapped exciton

References

1. Kim, J.; Park, J.; Park, B.; Kim, Y.; Park, B.; Park, S.H. Compact and Real-Time Radiation Dosimeter Using Silicon Photomultipliers for In Vivo Dosimetry in Radiation Therapy. *Sensors* **2025**, *25*, 857. https://doi.org/10.3390/s25030857.
2. Strigari, L.; Marconi, R.; Solfaroli-Camillocci, E. Evolution of Portable Sensors for In-Vivo Dose and Time-Activity Curve Monitoring as Tools for Personalized Dosimetry in Molecular Radiotherapy. *Sensors* **2023**, *23*, 2599. https://doi.org/10.3390/s23052599.
3. Kodama, S.; Kurosawa, S.; Morishita, Y.; Usami, H.; Torii, T.; Hayashi, M.; Sasano, M.; Azuma, T.; Tanaka, H.; Kochurikhin, V.; et al. Growth and Scintillation Properties of a New Red-Emitting Scintillator Rb_2HfI_6 for the Fiber-Reading Radiation Monitor. *IEEE Transactions on Nuclear Science* **2020**, *67*, 1055–1062. https://doi.org/10.1109/TNS.2020.2976695.
4. Bartram, R.H.; Kappers, L.A.; Hamilton, D.S.; Brecher, C.; Ovechkina, E.E.; Miller, S.R.; Nagarkar, V.V. Multiple Thermoluminescence Glow Peaks and Afterglow Suppression in CsI:Tl Co-Doped with Eu2+ or Yb2+. *IOP Conference Series: Materials Science and Engineering* **2015**, *80*, 012003. https://doi.org/10.1088/1757-899X/80/1/012003.
5. van Aarle, C.; Krämer, K.W.; Dorenbos, P. Lengthening of the Sm2+ 4f55d → 4f6 Decay Time through Interplay with the 4f6[5D0] Level and Its Analogy to Eu2+ and Pr3+. *Journal of Luminescence* **2024**, *266*, 120329. https://doi.org/10.1016/j.jlumin.2023.120329.
6. Wen, X.; Kucerkova, R.; Babin, V.; Prusa, P.; Kotykova, M.; Nikl, M.; Li, W.; Wang, Q.; Kurosawa, S.; Wu, Y. Scintillator-Oriented near-Infrared Emitting Cs4SrI6:Yb2+, Sm2+ Single Crystals via Sensitization Strategy. *Journal of the American Ceramic Society* **2023**, *106*, 6762–6768. https://doi.org/10.1111/jace.19302.
7. Alekhin, M.S.; Awater, R.H.P.; Biner, D.A.; Krämer, K.W.; de Haas, J.T.M.; Dorenbos, P. Luminescence and Spectroscopic Properties of Sm2+ and Er3+ Doped SrI2. *Journal of Luminescence* **2015**, *167*, 347–351. https://doi.org/10.1016/j.jlumin.2015.07.002.
8. Dixie, L.C.; Edgar, A.; Bartle, M.C. Spectroscopic and Radioluminescence Properties of Two Bright X-ray Phosphors: Strontium Barium Chloride Doped with Eu2+ or Sm2+ Ions. *Journal of Luminescence* **2014**, *149*, 91–98. https://doi.org/10.1016/j.jlumin.2013.12.061.

 doi:10.20944/preprints202504.2567.v1

9. Wolszczak, W.; Krämer, K.W.; Dorenbos, P. CsBa2I5:Eu2+,Sm2+—The First High-Energy Resolution Black Scintillator for γ-Ray Spectroscopy. *physica status solidi (RRL) – Rapid Research Letters* **2019**, *13*, 1900158. https://doi.org/10.1002/pssr.201900158.
10. Wolszczak, W.; Krämer, K.W.; Dorenbos, P. Engineering Near-Infrared Emitting Scintillators with Efficient $Eu^{2+} \rightarrow Sm^{2+}$ Energy Transfer. *Journal of Luminescence* **2020**, *222*, 117101. https://doi.org/10.1016/j.jlumin.2020.117101.
11. van Aarle, C.; Krämer, K.W.; Dorenbos, P. The Role of Yb2+ as a Scintillation Sensitiser in the Near-Infrared Scintillator CsBa2I5:Sm2+. *Journal of Luminescence* **2021**, *238*, 118257. https://doi.org/10.1016/j.jlumin.2021.118257.
12. Awater, R.H.P.; Alekhin, M.S.; Biner, D.A.; Krämer, K.W.; Dorenbos, P. Converting SrI2:Eu2+ into a near Infrared Scintillator by Sm2+ Co-Doping. *Journal of Luminescence* **2019**, *212*, 1–4. https://doi.org/10.1016/j.jlumin.2019.04.002.
13. Sofich, D.; Myasnikova, A.; Bogdanov, A.; Pankratova, V.; Pankratov, V.; Kaneva, E.; Shendrik, R. Crystal Growth and Spectroscopy of Yb2+-Doped CsI Single Crystal. *Crystals* **2024**, *14*, 500. https://doi.org/10.3390/cryst14060500.
14. Sofich, D.O.; Bogdanov, A.I.; Shendrik, R.Y. Spectroscopic and Vibrational Properties of CsI Single Crystals Doped with Divalent Samarium. *Optical Materials* **2025**, *162*, 116958. https://doi.org/10.1016/j.optmat.2025.116958.
15. Gektin, A.; Shiran, N.; Belsky, A.; Vasyukov, S. Luminescence Properties of CsI:Eu Crystals. *Optical Materials* **2012**, *34*, 2017–2020. https://doi.org/10.1016/j.optmat.2012.02.010.
16. Pankratova, V.; Kozlova, A.P.; Buzanov, O.A.; Chernenko, K.; Shendrik, R.; Šarakovskis, A.; Pankratov, V. Time-Resolved Luminescence and Excitation Spectroscopy of Co-Doped $Gd_3Ga_3Al_2O_{12}$ Scintillating Crystals. *Scientific Reports* **2020**, *10*, 20388. https://doi.org/10.1038/s41598-020-77451-x.
17. Pankratov, V.; Kotlov, A. Luminescence Spectroscopy under Synchrotron Radiation: From *SUPERLUMI* to *FINESTLUMI*. *Nuclear Instruments and Methods in Physics Research Section B: Beam Interactions with Materials and Atoms* **2020**, *474*, 35–40. https://doi.org/10.1016/j.nimb.2020.04.015.
18. Chernenko, K.; Kivimäki, A.; Pärna, R.; Wang, W.; Sankari, R.; Leandersson, M.; Tarawneh, H.; Pankratov, V.; Kook, M.; Kukk, E.; et al. Performance and Characterization of the FinEstBeAMS Beamline at the MAX IV Laboratory. *Journal of Synchrotron Radiation* **2021**, *28*, 1620–1630. https://doi.org/10.1107/S1600577521006032.
19. Rodriguez-Betancourtt, V.M.; Nattland, D. Raman Spectroscopic Study of Mixed Valence Neodymium and Cerium Chloride Solutions in Eutectic LiCl–KCl Melts. *Physical Chemistry Chemical Physics* **2005**, *7*, 173–179. https://doi.org/10.1039/B414757J.
20. Radzhabov, E.A. Spectroscopy of Divalent Samarium in Alkaline-Earth Fluorides. *Optical Materials* **2018**, *85*, 127–132. https://doi.org/10.1016/j.optmat.2018.08.044.
21. Suta, M.; Urland, W.; Daul, C.; Wickleder, C. Photoluminescence Properties of Yb^{2+} Ions Doped in the Perovskites $CsCaX_3$ and $CsSrX_3$ (X = Cl, Br, and I) – a Comparative Study. *Physical Chemistry Chemical Physics* **2016**, *18*, 13196–13208. https://doi.org/10.1039/C6CP00085A.
22. Zeng, P.; Cao, Z.; Chen, Y.; Yin, M. Investigation of the Temperature Characteristic in SrB4O7:Sm2+ Phosphor-in-Glass by Analyzing the Lifetime of 684 Nm. *Journal of Rare Earths* **2017**, *35*, 783–786. https://doi.org/10.1016/S1002-0721(17)60976-1.
23. Guzzi, M.; Baldini, G. Luminescence and Energy Levels of Sm2+ in Alkali Halides. *Journal of Luminescence* **1973**, *6*, 270–284. https://doi.org/10.1016/0022-2313(73)90023-9.
24. Shiran, N.; Gektin, A.; Boyarintseva, Y.; Vasyukov, S.; Boyarintsev, A.; Pedash, V.; Tkachenko, S.; Zelenskaya, O.; Zosim, D. Modification of NaI Crystal Scintillation Properties by Eu-doping. *Optical Materials* **2010**, *32*, 1345–1348. https://doi.org/10.1016/j.optmat.2010.04.014.
25. Shendrik, R.; Radzhabov, E. Absolute Light Yield Measurements on SrF_2 and BaF_2 Doped With Rare Earth Ions. *IEEE Transactions on Nuclear Science* **2014**, *61*, 406–410. https://doi.org/10.1109/TNS.2013.2290311.
26. Ucer, K.B.; Bizarri, G.; Burger, A.; Gektin, A.; Trefilova, L.; Williams, R.T. Electron Thermalization and Trapping Rates in Pure and Doped Alkali and Alkaline-Earth Iodide Crystals Studied by Picosecond Optical Absorption. *Physical Review B* **2014**, *89*, 165112. https://doi.org/10.1103/PhysRevB.89.165112.
27. Shendrik, R.; Radzhabov, E. Energy Transfer Mechanism in Pr-Doped SrF_2 Crystals. *IEEE Transactions on Nuclear Science* **2012**, *59*, 2089–2094. https://doi.org/10.1109/TNS.2012.2190146.

 doi:10.20944/preprints202504.2567.v1

28. Khanin, V.; Venevtsev, I.; Chernenko, K.; Pankratov, V.; Klementiev, K.; van Swieten, T.; van Bunningen, A.J.; Vrubel, I.; Shendrik, R.; Ronda, C.; et al. Exciton Interaction with Ce3+ and Ce4+ Ions in (LuGd)3(Ga,Al)5O12 Ceramics. *Journal of Luminescence* **2021**, *237*, 118150. https://doi.org/10.1016/j.jlumin.2021.118150.
29. Li, P.; Gridin, S.; Ucer, K.B.; Williams, R.T.; Del Ben, M.; Canning, A.; Moretti, F.; Bourret, E. Picosecond Absorption Spectroscopy of Excited States in BaBrCl with and without Eu Dopant and Au Codopant. *Physical Review Applied* **2019**, *12*, 014035. https://doi.org/10.1103/PhysRevApplied.12.014035.
30. Gektin, A.; Shiran, N.; Vasyukov, S.; Belsky, A.; Sofronov, D. Europium Emission Centers in CsI:Eu Crystal. *Optical Materials* **2013**, *35*, 2613–2617. https://doi.org/10.1016/j.optmat.2013.07.029.
31. Yakovlev, V.; Trefilova, L.; Karnaukhova, A.; Ovcharenko, N. Energy Transfer Mechanism in CsI:Eu Crystal. *Journal of Luminescence* **2014**, *148*, 274–276. https://doi.org/10.1016/j.jlumin.2013.12.020.
32. Hsu, O.L.; Bates, C.W. Excitonic Emission from CsI(Na). *Physical Review B* **1977**, *15*, 5821–5833. https://doi.org/10.1103/PhysRevB.15.5821.
33. Yakovlev, V.; Trefilova, L.; Meleshko, A.; Ovcharenko, N. Luminescence of Eu2+–Vc- Dipoles and Their Associates in CsI:Eu Crystals. *Journal of Luminescence* **2012**, *132*, 2476–2478. https://doi.org/10.1016/j.jlumin.2012.04.026.
34. Lushchik, Ch.; Lushchik, A. Evolution of Anion and Cation Excitons in Alkali Halide Crystals. *Physics of the Solid State* **2018**, *60*, 1487–1505. https://doi.org/10.1134/S1063783418080164.
35. Shalaev, A.A.; Shendrik, R.; Myasnikova, A.S.; Bogdanov, A.; Rusakov, A.; Vasilkovskyi, A. Luminescence of BaBrI and SrBrI Single Crystals Doped with Eu^{2+}. *Optical Materials* **2018**, *79*, 84–89. https://doi.org/10.1016/j.optmat.2018.03.017.
36. Lushchik, A.; Feldbach, E.; Kink, R.; Lushchik, Ch.; Kirm, M.; Martinson, I. Secondary Excitons in Alkali Halide Crystals. *Physical Review B* **1996**, *53*, 5379–5387. https://doi.org/10.1103/PhysRevB.53.5379.
37. Sisodiya, D.S.; Singh, S.G.; Chandrakumar, K.R.S.; Patra, G.D.; Ghosh, M.; Pitale, S.; Sen, S. Optimizing the Scintillation Kinetics of CsI Scintillator Single Crystals by Divalent Cation Doping: Insights from Electronic Structure Analysis and Luminescence Studies. *The Journal of Physical Chemistry C* **2024**, *128*, 197–209. https://doi.org/10.1021/acs.jpcc.3c06098.
38. Brecher, C.; Lempicki, A.; Miller, S.R.; Glodo, J.; Ovechkina, E.E.; Gaysinskiy, V.; Nagarkar, V.V.; Bartram, R.H. Suppression of Afterglow in CsI:Tl by Codoping with Eu2+—I: Experimental. *Nuclear Instruments and Methods in Physics Research Section A: Accelerators, Spectrometers, Detectors and Associated Equipment* **2006**, *558*, 450–457. https://doi.org/10.1016/j.nima.2005.11.119.
39. Bartram, R.H.; Kappers, L.A.; Hamilton, D.S.; Lempicki, A.; Brecher, C.; Glodo, J.; Gaysinskiy, V.; Ovechkina, E.E. Suppression of Afterglow in CsI:Tl by Codoping with Eu2+—II: Theoretical Model. *Nuclear Instruments and Methods in Physics Research Section A: Accelerators, Spectrometers, Detectors and Associated Equipment* **2006**, *558*, 458–467. https://doi.org/10.1016/j.nima.2005.11.051.
40. Shahmaleki, S.; Rahmani, F. Scintillation Properties of CsI(Tl) Co-Doped with Tm2+. *Radiation Physics and Engineering* **2021**, *2*, 13–19. https://doi.org/10.22034/rpe.2021.295907.1032.
41. Takase, S.; Miyazaki, K.; Nakauchi, D.; Kato, T.; Kawaguchi, N.; Yanagida, T. Development of Nd-doped CsI Single Crystal Scintillators Emitting near-Infrared Light. *Journal of Luminescence* **2024**, *267*, 120400. https://doi.org/10.1016/j.jlumin.2023.120400.